UC Irvine

UC Irvine Previously Published Works

Title

IKs channels open slowly because KCNE1 accessory subunits slow the movement of S4 voltage sensors in KCNQ1 pore-forming subunits

Permalink

https://escholarship.org/uc/item/6p29c29q

Journal

Proceedings of the National Academy of Sciences of the United States of America, 110(7)

ISSN

0027-8424

Authors

Ruscic, Katarina J
Miceli, Francesco
Villalba-Galea, Carlos A
et al.

Publication Date

2013-02-12

DOI

10.1073/pnas.1222616110

Copyright Information

This work is made available under the terms of a Creative Commons Attribution License, availalbe at https://creativecommons.org/licenses/by/4.0/

Peer reviewed

eScholarship.org Powered by the California Digital Library
University of California

I_{Ks} channels open slowly because KCNE1 accessory subunits slow the movement of S4 voltage sensors in KCNQ1 pore-forming subunits

Katarina J. Ruscic[a,b], Francesco Miceli[b,1], Carlos A. Villalba-Galea[b,2], Hui Dai[a], Yukiko Mishina[b,3], Francisco Bezanilla[b,4], and Steve A. N. Goldstein[a,b,4]

[a]Department of Biochemistry, Brandeis University, Waltham, MA 02454; and [b]Department of Pediatrics and Department of Biochemistry and Molecular Biology, University of Chicago, Chicago, IL 60637

Contributed by Francisco Bezanilla, December 26, 2012 (sent for review November 22, 2012)

Human I_{Ks} channels activate slowly with the onset of cardiac action potentials to repolarize the myocardium. I_{Ks} channels are composed of KCNQ1 (Q1) pore-forming subunits that carry S4 voltage-sensor segments and KCNE1 (E1) accessory subunits. Together, Q1 and E1 subunits recapitulate the conductive and kinetic properties of I_{Ks}. How E1 modulates Q1 has been unclear. Investigators have variously posited that E1 slows the movement of S4 segments, slows opening and closing of the conduction pore, or modifies both aspects of electromechanical coupling. Here, we show that Q1 gating current can be resolved in the absence of E1, but not in its presence, consistent with slowed movement of the voltage sensor. E1 was directly demonstrated to slow S4 movement with a fluorescent probe on the Q1 voltage sensor. Direct correlation of the kinetics of S4 motion and ionic current indicated that slowing of sensor movement by E1 was both necessary and sufficient to determine the slow-activation time course of I_{Ks}.

Kv7.1 | MinK | site-directed fluorimetry | heart | arrhythmia

E1 and Q1 subunits assemble to form I_{Ks} potassium channels in the heart and ear (1–6). Demonstrating that both subunits are required for normal physiology, inherited mutations in either subunit that decrease expression level or alter function can cause life-threatening cardiac arrhythmias and deafness (7, 8). The mechanism by which E1 alters the biophysical parameters of Q1 to produce I_{Ks} channel currents is the subject of active debate.

Q1 (also Kv7.1) is similar to other voltage-gated potassium (Kv) channel α-subunits in having six transmembrane spans (Fig. 1*A*): S1–S4 form the voltage sensor domain (VSD), and S5–S6 carry a reentrant, pore-forming (P) loop. Like other Kv channels, four Q1 subunits create a single, central ion conduction pore (9). Activation of Kv channels occurs when membrane depolarization induces positively charged residues in the S4 segments to move outward relative to counter charges in the S2 and S3 segments. This movement is coupled to opening of the ion conduction pore. Q1 is notable because the S4 segments are charge-poor compared with other Kv channel α-subunits (10).

E1 (also MinK) is one of a family of five related β-subunits with a single transmembrane span (11) (Fig. 1*A*) that assemble with many Kv channel subunits (12–14). I_{Ks} channels have been shown to carry two E1 subunits (9, 15, 16), although the notion of variable subunit stoichiometry has been revived in a study using low levels of E1 (17). Compared with channels formed only with Q1, E1 incorporation has been demonstrated to slow activation and deactivation kinetics, hyperpolarize the voltage-dependence of activation, suppress inactivation, increase single-channel conductance, and alter ion selectivity and open-channel pore block (2, 6, 18–23). E1 has therefore been hypothesized to interact with both the pore and VSD in I_{Ks} channels (24–26).

Two prior studies designed to identify the channel domain where E1 acts to slow I_{Ks} activation yielded contradictory results, despite using the same, albeit indirect, assay. In both studies, I_{Ks} channels carrying Q1 subunits mutated to encode Cys residues in and near the S4 span were exposed to methanethiosulfonate (MTS) reagents from the external solution to assess voltage-dependent exposure of the altered sites; in one case, E1 was determined to slow S4 accessibility (27) and in the other, E1 was proposed to impede pore opening (28). More recently, a fluorometric study argued that E1 has both effects (29).

Here, we use direct, simultaneous, real-time electrophysiological and optical measurements of movement of the Q1 voltage sensors: the first method assesses gating charges moving in the membrane electric field (30) using the cut-open oocyte voltage clamp (COVC) technique (31); the second approach records ion currents traversing the pore and concurrently applies site-directed fluorimetry (SDF), wherein a probe bound to the S4 reports on changes in its local environment (32). In the absence of E1, we were able to measure Q1 channel gating charge movements, observing them to be ∼28-fold slower than those in Shaker channels at 40 mV and 28 °C. Gating currents were not resolved with E1 because S4 movement was too slow, a finding demonstrated using SDF and a fluorescent probe on the Q1 voltage sensor.

Significance

E1 and Q1 protein subunits assemble to form I_{Kslow} channels in the heart and ear. Inherited mutations in either subunit that decrease protein level or alter function can cause life-threatening cardiac arrhythmias and deafness. The mechanism by which E1 slows channel opening has been the subject of active debate. Here, we use gating current measurements and simultaneous recordings of ionic currents and changes in fluorescence of a probe on the Q1 voltage sensors to demonstrate that E1 slows the movement of sensors in a manner that is both necessary and sufficient to determine the slow activation time course of I_{Ks} channels.

Author contributions: F.B. and S.A.N.G. designed research; K.J.R., F.M., C.A.V.-G., H.D., and Y.M. performed research; F.B. contributed new reagents/analytic tools; K.J.R. analyzed data; and K.J.R., F.B., and S.A.N.G. wrote the paper.

The authors declare no conflict of interest.

Freely available online through the PNAS open access option.

[1]Present address: Section of Pharmacology, Department of Neuroscience, University of Naples Federico II, 80131 Naples, Italy.

[2]Present address: Department of Physiology and Biophysics, Virginia Commonwealth University, Richmond, VA 23298.

[3]Present address: Centre of Global Communication Strategies, The University of Tokyo College of Arts and Sciences, 3-8-1 Komaba, Meguro-Ku, Tokyo 153-8902, Japan.

[4]To whom correspondence may be addressed. E-mail: fbezanilla@uchicago.edu or goldstein@brandeis.edu.

This article contains supporting information online at www.pnas.org/lookup/suppl/doi:10.1073/pnas.1222616110/-/DCSupplemental.

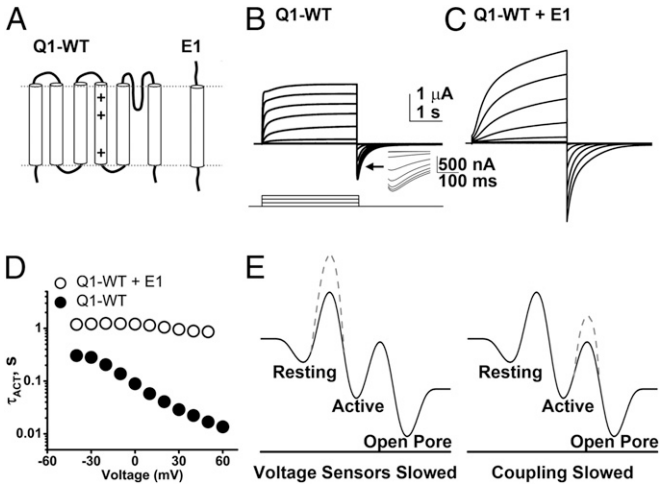

Fig. 1. E1 subunits alter the biophysical properties of Q1-WT channels. E1 subunits slow the kinetics of Q1-WT channels and augment current magnitude. Currents were studied in cells expressing the indicated subunits using 3-s test pulses between −90 and 60 mV from a holding potential of −90 mV via COVC at 28 °C. (*A*) Secondary structure of Q1-WT indicating the positively charged residues in the S4 segment (+). E1 is a single membrane pass subunit. (*B*) Family of ionic currents from a cell expressing Q1-WT channels shown in 20-mV intervals. (*Inset*) A magnified view of the tail current hook. (*C*) Family of currents evoked from a cell expressing Q1-WT + E1, pulse protocol as in *B*. (*D*) Activation time-constants (τ_{ACT}) for Q1-WT (●) and Q1-WT + E1 channels (○) show that E1 slows activation of Q1-WT channels across the voltage range studied. Mean ± SEM for six to seven cells per group; error bars are smaller than symbols. (*E*) Simplified energy landscape for Q1-WT channel gating kinetics with a single transition of voltage sensors from the resting to active state, and barrier between the active voltage sensor state and pore opening. The black lines correspond to Q1-WT channels. The dashed lines indicate energy barriers raised by assembly with E1 to form I_{Ks} channels. (*Left*) A model whereby E1 raises the energy barrier for voltage-sensor transitions between resting and active states, slowing voltage-sensor movement. (*Right*) A model whereby E1 raises the energy barrier between voltage-sensor activation and pore opening.

Results

E1 Subunits Alter the Biophysical Properties of Q1-WT Channels. First, wild-type KCNQ1 channels (Q1-WT) were characterized using COVC at 28 °C (Fig. 1*B*). When expressed alone, Q1-WT ionic currents activated at potentials more depolarized than −60 mV (Fig. S1*A*) and showed partial inactivation during the test pulse as revealed by a "hook" in the tail currents, indicative of recovery from inactivation (Fig. 1*B*, *Inset*) (21). Expression of Q1-WT with E1 to form I_{Ks} channels led to an increase in the magnitude of whole-cell currents, suppressed inactivation, and shifted the voltage required to activate the current (Fig. 1*C* and Fig. S1*A*). Thus, the half-maximal activation voltage ($V_{1/2}$) determined from the normalized *G-V* relationships was depolarized with E1 by ∼40 mV from −24 mV to 23 mV (Table 1 and Fig. S1*A*). Furthermore, E1 slowed the kinetics of channels, prolonging both the voltage-dependent activation and deactivation (Fig. 1*D*, Fig. S1*B*, and Table 1). At 40 mV, τ_{ACT} and τ_{DEACT} of Q1-WT channels were 0.02 ± 0.002 s and 0.11 ± 0.02 s (n = 6), and this was slowed by E1 ∼40-fold and ∼2-fold, respectively, to 0.9 ± 0.07 s and 0.20 ± 0.03 s for I_{Ks} channels (n = 7) (Fig. 1*D* and Fig. S1*B*).

To determine if E1 altered the biophysical properties of the channels by slowing the motion of the Q1 voltage sensors or by slowing opening of the channel pore (Fig. 1*E*), we pursued direct measurements of S4 segment movements in the presence and absence of expressed E1.

Q1-WT Gating Charge Moves Slowly and Is Not Resolved with Coexpression of E1. COVC and potassium depletion allowed recording of transient time- and voltage-dependent currents for Q1-WT channels corresponding to ON and OFF gating currents, I_{gON} and I_{gOFF}, respectively (Fig. 2*A*). I_{gON} for Q1-WT rose abruptly, similarly to Q4 channels (33), and unlike Shaker channels that showed a distinct rising phase in response to large depolarizing pulses before exponentially decreasing (Fig. S2*A*) (34). I_{gON} for Q1-WT was notably slower than for Q4 and Shaker channels, an observation highlighted by normalizing Q_{ON} for the three channels to 1 nC of gating charge (Fig. 2*B*). I_{gON} at 40 mV for Q1-WT is ∼fourfold slower than Q4 channels and ∼28-times slower than Shaker channels (Table 1 and Fig. S2*B*).

The slow kinetics of Q1-WT gating currents made them challenging to measure, with average peak I_{gON} of 41.7 ±7 nA at 40 mV (n = 7). In contrast, peak I_{gON} for Shaker channels under the same conditions was 838 ± 286 nA (n = 6) (Fig. S2*B*). The magnitude of Q1-WT gating charge scaled with the initial level of ionic current in the cell before potassium depletion (Fig. 2*C*) was ∼0.7 nC/μA of initial potassium current at 40 mV.

Gating currents could not be resolved for channels formed from Q1-WT + E1 subunits (Fig. 2*B* and Fig. S2*A*), despite current density before potassium depletion that was ∼sevenfold greater than for Q1-WT channels. This finding was consistent with E1-induced reduction in the signal below our experimental resolution because of the slowing of gating kinetics.

Table 1. Ionic and gating current parameters for channels studied

Channel	Protocol	$V_{1/2}$ (mV)	z, e-	τ_{ACT} (ms)	τ_{DEACT} (ms)
Q1-WT	Ionic 3 s	−23.7 ± 1.4	2.44 ± 0.10	22.3 ± 1.9 16.8 ± 1.5*	109.4 ± 15.9†
Q1-WT + E1	Ionic 3 s	22.5 ± 1.2	2.11 ± 0.08	887 ± 74 860 ± 73*	192.8 ± 27.7†
Q1-WT	Ionic 300 ms	−8.1 ± 0.8	1.61 ± 0.04	29.9 ± 2.9	63.5 ± 5.2
Q1-WT	Gating 300 ms	−22.7 ± 1.0	2.19 ± 0.16	22.8 ± 1.5	75.7 ± 7.8
Shaker	Gating 60 ms	−42.4 ± 1.1	3.73 ± 0.31	0.8 ± 0.1	2.6 ± 0.2
KCNQ4	Gating 70 ms	−23.8 ± 0.6	2.09 ± 0.06	5.9 ± 0.2	18.2 ± 2.2
Q1-H240R	Ionic 150 ms	−21.5 ± 1.2	1.37 ± 0.06	15.3 ± 0.7	158.2 ± 11.1
Q1-H240R	Gating 150 ms	−35.8 ± 2.8	1.83 ± 0.27	16.0 ± 2.8	318.2 ± 70.3
Q1-H240R + E1	Ionic 3 s	10.3 ± 2.2	1.31 ± 0.06	688 ± 18	1,754 ± 239†

Ionic and gating currents were studied using the protocols described in *Materials and Methods*. The duration of the test pulse is noted. Data were fit to the equation for *G* as per *Materials and Methods*. Activation and deactivation kinetics, determined from single-exponential fits, are reported as the activation time-constant, τ_{ACT} at 40 mV (for Q1-WT and Q1-WT + E1 activation at 50 mV is also shown, *) and deactivation time-constant, τ_{DEACT} at −100 mV, or at −90 mV (where indicated, †). Data are mean ± SEM for three to seven cells.

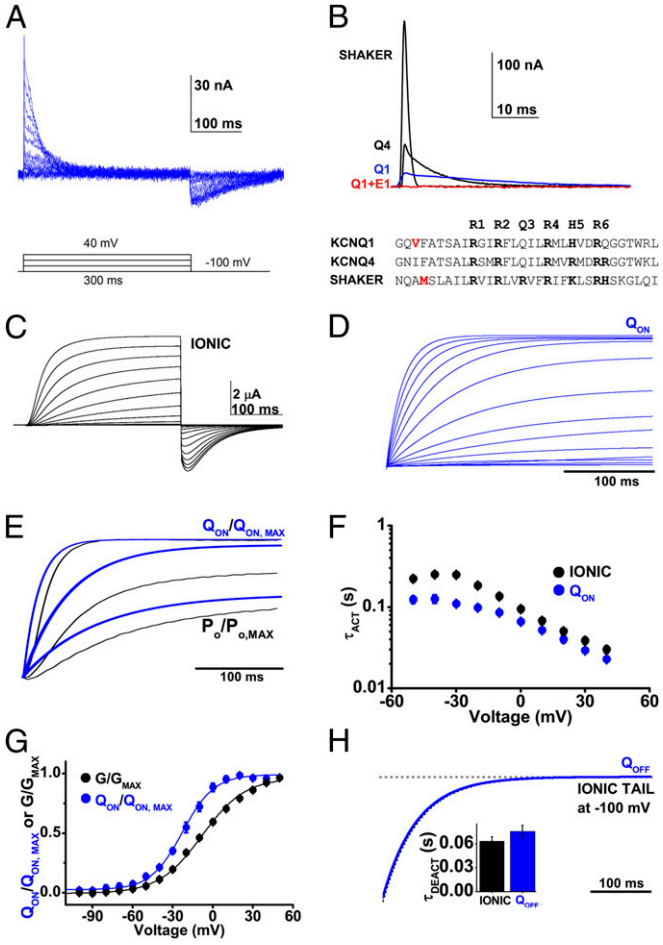

Fig. 2. Q1-WT gating charge activates slowly but precedes ionic current. Q1-WT ionic and gating currents were recorded using 300-ms test pulses. Ionic currents were measured without potassium depletion, in external solution containing 4 mM potassium. Data are mean ± SEM for six to seven cells in each group. (*A*) Representative family of Q1-WT gating currents evoked using the voltage protocol indicated with 10-mV intervals. (*B*) Superposition of gating currents evoked at 40 mV from cells expressing Shaker, KCNQ4 (Q4), Q1-WT (Q1, blue), or Q1-WT + E1 channels (Q1 + E1, red), normalized to 1-nC gating charge. The aligned amino acid sequences of the S4 segments of Q1-WT, Q4, and Shaker channels are shown. The Q1 V221C labeling site and the commonly used labeling site in Shaker are indicated in red. (*C*) A representative family of Q1-WT ionic currents using the same pulse protocol as in *A*. (*D*) Exemplar integrated gating current (Q_{ON}) from −100 to 40 mV, ΔV 10 mV. (*E*) Representative example of normalized superposition of Q_{ON} (blue) and open probability (black) activation at 40, 0, and −20 mV. (*F*) Mean activation time-constant (τ_{ACT}) for Q1-WT channel Q_{ON} (blue) and ionic current (black) measured over the voltages indicated. (*G*) Mean, normalized *Q-V* and *G-V* relationships measured after 300 ms and fit as described in *Materials and Methods*; determined values are in Table 1. (*H*) Superposition of an example integrated OFF-gating current, Q_{OFF}, (blue), and deactivation of ionic current (black) at −100 mV from a 40-mV test pulse. (*Inset*) Mean τ_{DEACT}.

Q1-WT Gating Charge Movement Precedes and Tracks Ionic Current. Measuring ionic currents from cells expressing Q1-WT with the same protocol used to assess gating currents revealed that integrated gating charge movement (Q_{ON}) preceded pore opening (normalized P_o) (Fig. 2 *D* and *E*). Comparing the activation time course of Q_{ON} and ionic current showed that although gating-charge movement precedes ionic currents across the voltage-range studied, kinetics of the two parameters were correlated, consistent with a channel that requires voltage-dependent gating-charge movement before pore opening (Fig. 2*F* and Table 1). Moreover, $V_{1/2}$ for Q_{ON} determined from normalized Q_{ON}-*V* curves was hyperpolarized with respect to the *G-V* relationship for Q1-WT by 15 mV, indicating that gating charges move at potentials more hyperpolarized than those that open the channel pore (Fig. 2*G* and Table 1).

Similar to studies of Q4 channels (33) and Shaker channels (Fig. S2*A*), I_{gOFF} measured for Q1-WT was lower in amplitude than I_{gON} because deactivation of voltage sensors at −100 mV is slower than activation at +40 mV (Fig. 2*A*). Consistent with prior studies of Shaker channels (34, 35), the mean τ for Q1-WT Q_{OFF} was slower than ionic current deactivation, 0.076 ± 0.008 compared with 0.064 ± 0.005 s (n = 6–7) (Fig. 2*H* and Table 1).

Mutant Q1-H240R Shows Hyperpolarized Ionic and Gating Current Activation. Q1-WT channels have a His residue at position 240, corresponding to a site where Shaker has its fifth S4 segment charge (K5), and Q4 has its fourth Arg (Fig. 2*B*). Mutation of Q1 from His to Arg at 240 (Q1-H240R) recapitulates the charge pattern in Q4 (Fig. 2*B*), and has been shown by others to shift the *G-V* relationship to more hyperpolarized potentials (10). This construct was produced in the first instance to determine if failure to resolve gating currents with Q1-WT + E1 channel was a consequence of S4 charge paucity compared with Q4.

As expected, the $V_{1/2}$ of the normalized Q_{ON}-*V* and *G-V* relationships for Q1-H240R were both hyperpolarized with respect to Q1-WT by ∼13 mV (Table 1). Of note, the mutation slowed I_{gOFF} and τ_{DEACT} kinetics by ∼4.2- and 2.5-fold, respectively, compared with Q1-WT (Fig. 3*A* and Table 1). Superimposing normalized Q_{ON} and P_o traces demonstrated that like Q1-WT, gating charge movement preceded opening of the Q1-H240R conduction pore (Fig. 3*B*). Also like Q1-WT, τ_{ACT} for Q1-H240R ionic current, and Q_{ON} had similar values at depolarized potentials (Fig. 3*C*) and $V_{1/2}$ of the normalized Q_{ON}-*V* relationship of Q1-H240R channels was hyperpolarized with respect to the *G-V* relationship by 14 mV, consistent with movement of voltage sensors before pore opening (Fig. 3*D* and Table 1). Kinetics of I_{gON} and conductance activation at 40 mV were ∼1.4-fold and 2-fold faster than in Q1-WT, but peak I_{gON} of Q1-H240R at 40 mV was slightly lower than for Q1-WT at 24.3 ± 2.2 nA.

The $V_{1/2}$ of Q1-H240R + E1 channel activation was also hyperpolarized by 12 mV, compared with currents with wild-type subunits (Table 1 and Fig. S3). Despite activation at more hyperpolarized potentials and larger current density before potassium depletion than that recorded for Q1-H240R channels, gating currents could not be resolved when E1 subunits were also expressed (Fig. S3*B*).

Q1-F S4 Movements Measured by Fluorimetry Precede and Correlate with Ionic Current. Movement of the S4 segment in Kv channels can be tracked by SDF, a technique based mostly on quenching and dequenching of a fluorescent probe covalently bonded to the voltage sensor. To perform SDF, we introduced a Cys residue at sequential sites in the external S3-S4 linker of Q1 to allow labeling with tetramethylrhodamine-5-maleimide (TMRM) (and removed two native Cys residues at 214 and 331 by mutation to Ser to mitigate confounding fluorescence signals). The mutant that operated most like Q1-WT had a target Cys in place of Val221, was identified as Q1-F, and studied further (Fig. 2*B*).

Q1-F channels had a $V_{1/2}$ of activation that was hyperpolarized by 34 mV with respect to Q1-WT (Table 2) but maintained other biophysical hallmarks, including inactivation observed as a hook in the tail current (Fig. 4*A*). To mitigate the impact of the shift in $V_{1/2}$, Q1-F channels were studied with a prepulse to −120 mV; nonetheless, some channels were open at the start of each test pulse (Fig. 4*A*).

Fluorescent signals were recorded simultaneously with ionic currents from cells expressing Q1-F channels (Fig. 4 *A* and *B*).

Table 2. Simultaneous ionic and SDF parameters for channels studied

Channel	Protocol	$V_{1/2}$ (mV)	z, e-	τ_{ACT} (ms)	τ_{DEACT} (ms)
Q1-F	Ionic 3 s	−58.1 ± 1.3	1.27 ± 0.07	30.0 ± 2.7	347.3 ± 44.8* 438.3 ± 54.2
Q1-F	Fluorescence 3 s	−82.1 ± 2.7	2.05 ± 0.24	27.7 ± 2.8	451.7 ± 51.7* 508.8 ± 68.2
Q1-F + E1	Ionic 3 s	19.5 ± 0.8	1.22 ± 0.03	917 ± 68	1842 ± 244
Q1-F + E1	Fluorescence 3 s	19.3 ± 1.5	1.19 ± 0.07	937 ± 40	1971 ± 231
Q1-F-H240R	Ionic 3 s	−74.8 ± 1.9	1.31 ± 0.10	N/A	965.1 ± 71.9*
Q1-F-H240R	Fluorescence 3 s	−84.8 ± 0.9	2.14 ± 0.12	N/A	486.7 ± 44.0*
Q1-F-H240R†	Ionic 3 s	−65.6 ± 3.2	1.03 ± 0.09	N/A	719.7 ± 154*
Q1-F-H240R†	Fluorescence 3 s	−78.06 ± 1.4	1.68 ± 0.14	N/A	524.8 ± 75.6*
Q1-F-H240R†	Ionic 300 ms	N/A	N/A	34.5 ± 3.7‡ 30.77 ± 4.1‡§	N/A
Q1-F-H240R†	Fluorescence 300 ms	N/A	N/A	29.0 ± 2.3‡ 26.49 ± 2.3‡§	N/A
Q1-F-H240R + E1	Ionic 3 s	17.5 ± 1.1	1.06 ± 0.03	905 ± 89§	1,415 ± 203
Q1-F-H240R + E1	Fluorescence 3 s	5.8 ± 0.6	0.95 ± 0.01	835 ± 49§	1,501 ± 276

The channels were studied by COVC and SDF recording as described in the *Materials and Methods*. The duration of the test pulse is indicated. $V_{1/2}$, the voltage of half-maximal activation and *z*, the effective valance, were derived as described in Table 1. The activation time-constant, τ_{ACT} is reported at 40 mV (or 50 mV where indicated, §) from a prepulse to −120 mV (or −160 mV where indicated, ‡), and using 2 mM external $CaCl_2$ (or 20 mM as indicated, †). Deactivation time-constant, τ_{DEACT} at −90 mV (or −120 mV where indicated, *). τ_{DEACT} for Q1-F-H240R were fit by a double exponential and a weighted average of both τ is reported. Data are mean ± SEM for three to seven cells.

Superposition of the normalized traces revealed that like gating current in Q1-WT, fluorescent signals reflecting movement of the S4 segment in Q1-F preceded the activation of ionic current (Fig. 4*C*). Fluorescence had two components an order of magnitude different in speed, which we isolated by fitting the data with two exponentials (Fig. S4). Ionic current and the fast kinetic component of the change in fluorescence had similar activation kinetics (Fig. 4*D*).

The *F-V* relationship of Q1-F channels was hyperpolarized with respect to the *G-V* by 24 mV (Fig. 4*E* and Table 2), indicating that during a depolarizing stimulus the S4 segment will move before the pore opens. In contrast, SDF signals demonstrate that the S4 conformational changes that correspond to deactivation are ∼1.3-fold slower than pore closure (Fig. 4*F* and Table 2).

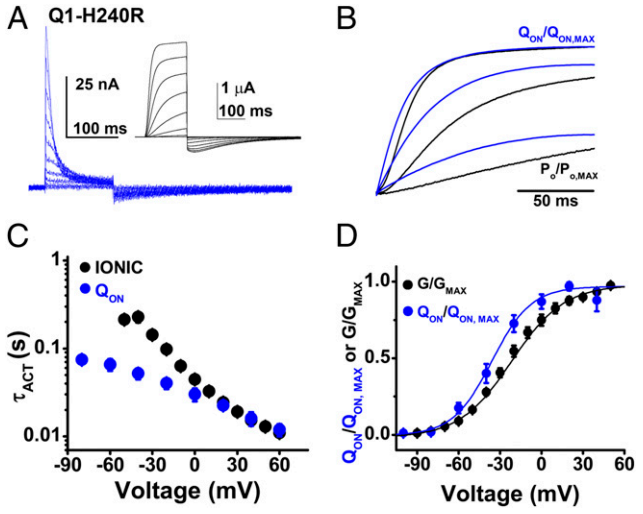

Fig. 3. Q1-H240R channel ionic and gating currents are hyperpolarized compared to Q1-WT. Ionic currents and gating currents for Q1-H240R channels were measured using COVC at 28 °C with the protocol in Fig. 2 with 150-ms test pulses. Data are means ± SEM for three to six cells in each group. (*A*) Representative family of gating currents from −100 to 60 mV, shown in 20-mV intervals for clarity. (*Inset*) A representative family of ionic currents using the same pulse protocol. (*B*) Representative superposition of normalized ON-gating charge (Q_{ON}, blue) and open probability (P_O, black) at 40, 0, and −40 mV. (*C*) Mean activation time-constants (τ_{ACT}) for ionic current (black) and Q_{ON} (blue) plotted against the test potential studied. (*D*) Mean, normalized *Q-V* and *G-V* relationships measured after 150 ms and fit as described in Fig. 2; determined values are in Table 1.

Barium Blocks Q1-F Channels but Does Not Alter Voltage Sensor Activation. To demonstrate that fluorescent signals obtained from Q1-F channels were insensitive to barium at the levels used in studies of gating currents and that pore blockade did not alter S4 movements, ionic currents and SDF signals were recorded simultaneously from cells expressing Q1-F in the presence of 2 mM external barium (Fig. S5*A*). Although 2 mM barium slowed τ_{ACT} of Q1-F ionic currents by nearly an order of magnitude, τ_{ACT} of fluorescent signals were unaffected (Fig. S5*B*). Similarly, the normalized *F-V* relationship of Q1-F channels was unaltered by 2 mM external barium, but the $V_{1/2}$ for voltage-dependent conductance was depolarized by >90 mV (Fig. S5*C*). Thus, barium impacts the activation kinetics and voltage-dependence of ionic current via pore blockade but does not alter sensor activation.

SDF Shows That E1 Slows Voltage Sensor Movement. E1 modified the operation of Q1-F as it did Q1-WT: activation was slowed, $V_{1/2}$ of activation was depolarized and inactivation was suppressed (Table 2). Ionic current and fluorescent signals from E1 + Q1-F channels were recorded simultaneously (Fig. 5 *A* and *B*). When the normalized traces were superimposed, S4 movement preceded pore opening with E1 (Fig. 5*C*) as with Q1-F alone (Fig. 4*C*). Furthermore, E1 did not change the close correlation of kinetics of current activation and S4 movement (Fig. 5*D*). In contrast, E1 slowed τ_{ACT} for both ionic current activation and the change in the fluorescent signal by ∼30-fold compared with Q1-F alone (Table 2). Whereas I_{Ks} activation kinetics vary from oocyte to oocyte, simultaneous SDF recording in the same cell revealed that the kinetics of ionic current activation and the change in the fluorescent signal matched (Fig. S6).

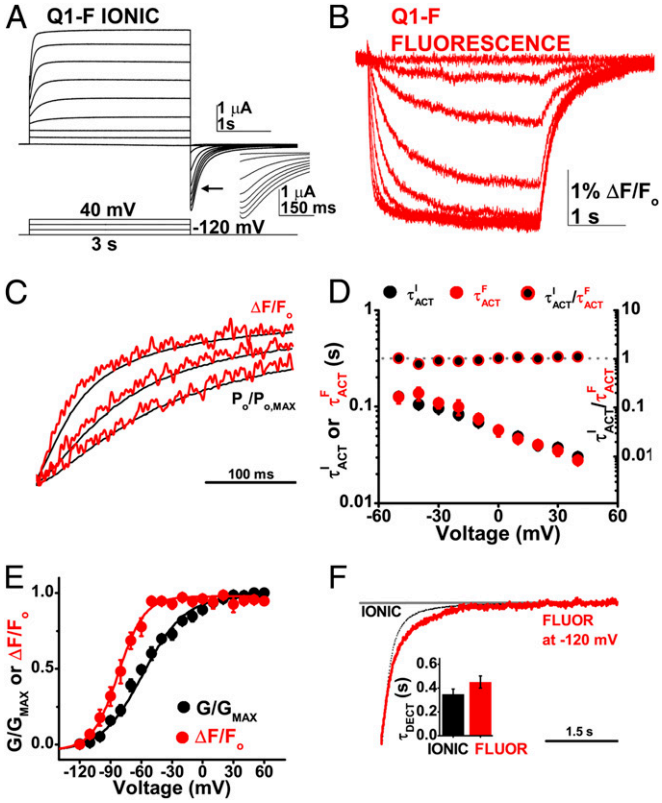

Fig. 4. Q1-F voltage sensor movements measured by SDF precede ionic current. Ionic current and fluorescence signals were studied simultaneously at 28 °C in cells expressing Q1-F channels. Data are means ± SEM for six to seven cells per group. (*A*) Representative family of ionic currents recorded from a cell expressing Q1-F channels using the protocol indicated, with a 1-s −120 mV prepulse, −120 mV tail, and −90 mV holding potential. (*Inset*) The hooked tail current characteristic of Q1 channel inactivation. Currents are shown in 20-mV intervals for clarity. (*B*) Family of fluorescence measurements in the same cell as in *A*, recorded simultaneously. (*C*) Normalized superposition of Q1-F fluorescence signals ($\Delta F/F_O$, red) and ionic current ($P_O/P_{O,\,MAX}$, black) evoked by test pulses to 40, 0, and −20 mV for an example cell. Ionic current is normalized by the tail conductance to reflect relative open probability with respect to time. (*D*) Activation time-constant for Q1-F fluorescence signals (τ^F_{ACT}, red circles) and ionic current (τ^I_{ACT}, black circles) in seconds, left axis. Mean ratios of τ^I_{ACT} to τ^F_{ACT} (black/red circles; right axis). The ratio is close to 1 (dotted gray line; right axis) over the voltage range studied. (*E*) Mean, normalized fluorescence (F, red) and conductance (G, black)-voltage relationships measured at 3 s and fit as in Fig. 2; determined values are in Table 2. (*F*) Superposition of ionic current deactivation (dotted black line) and fluorescence (red line) at −120 mV from a 40-mV test pulse. (*Inset*) Mean deactivation time-constants, τ_{DEACT} for fluorescence (red) and ionic tail current (black) at −120 mV.

As expected from studies of E1 + Q1-WT, neither the *F-V* nor the *G-V* relationships for E1 + Q1-F channels saturated after a 3-s test pulse (Fig. 5 *A* and *B*), and the isochronal $V_{1/2}$ was depolarized at least 77 mV compared with Q1-F alone (Fig. 5*E* and Table 2). Also in accord with expectations, E1 slowed both ionic tail current deactivation and fluorescence deactivation ~fourfold. (Fig. 5*F* and Table 2).

E1 Also Slows the Movement of Q1-F-H240R Voltage Sensors. Our inability to measure gating currents for channels with Q1-H240R and E1 suggested, as for Q-WT, that E1 voltage sensor movement was slowed. To confirm this with SDF, we studied Q1-F-H240R. Channels with Q1-F-H240R subunits activated at potentials more hyperpolarized than those with Q1-H240R (Tables 1 and 2); therefore, a hyperpolarizing prepulse to −160 mV was required to increase the proportion of channels closed before the test pulse and 20 mM external calcium was added to right-shift the *G-V* curve when measuring activation kinetics (Fig. S7 *C–E*). With respect to Q1-F channels, *F-V* and *G-V* relationships for Q1-F-H240R were hyperpolarized by ~3 mV and ~17 mV, respectively (Fig. 6 and Table 2). Simultaneous measurement of ionic current and fluorescence signals from cells expressing Q1-F-H240R showed that E1 slowed S4 movement (Fig. 6). As for Q1-F, normalized superposition of ionic currents and fluorescent signals for Q1-F-H240R demonstrated that pore opening and sensor movement occurred with similar kinetics (Fig. S7 *F* and *G*) and, although E1 did not alter the high correlation between activation kinetics of current and SDF, it slowed τ_{ACT} for both ~30-fold (Fig. S7*H*). E1 slowed τ_{DEACT} ~threefold (Table 2). Thus, slowing of the voltage sensor movement by E1 in Q1-F-H240R, a mutant with a hyperpolarized *G-V* relationship, was sufficient to explain slowed activation, just as for Q1-F.

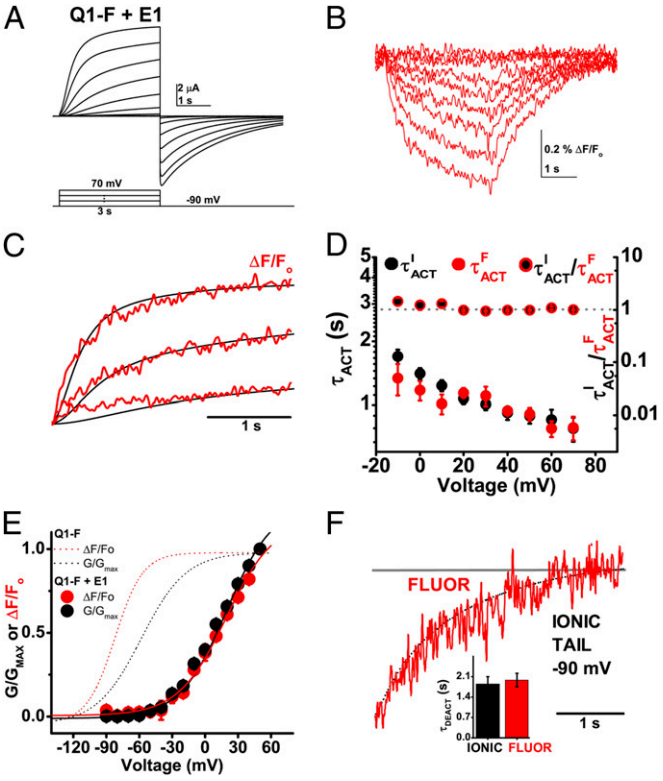

Fig. 5. E1 slows the voltage sensors of Q1-F channels. Ionic current and fluorescence signals were studied simultaneously at 28 °C in cells expressing Q1-F + E1 channels. Data are means ± SEM for six to seven cells per group. (*A*) Representative family of ionic currents recorded from a cell expressing Q1-F + E1 channels using the protocol indicated and shown in 20-mV intervals for clarity. (*B*) Representative family of fluorescence traces from the same cell shown in *A*. (*C*) Normalized superposition of Q1-F + E1 fluorescence signals ($\Delta F/F_O$, red) and ionic current ($P_O/P_{O,\,MAX}$, black) evoked by test pulses to 70, 30, and −10 mV measured simultaneously for a representative cell. (*D*) The activation time-constant for Q1-F + E1 fluorescence signals (τ^F_{ACT}, red circles) and ionic current (τ^I_{ACT}, black circles) in seconds, left axis. Mean ratios of τ^I_{ACT} to τ^F_{ACT} (black/red circles; right axis). The ratio is ~1 (dotted gray line; right axis) over the voltages studied. (*E*) Mean, normalized fluorescence (F, red) and conductance (G, black) –voltage relationships for Q1-F + E1 measured at 3 s and fit as in Fig. 2; determined values are in Table 2. The normalized *F* and *G* for Q1-F (red and black dotted lines, respectively) from Fig. 4 are included for reference. (*F*) Superposition of exemplar ionic current deactivation (dotted black line) and fluorescence (red line) at −120 mV from a 40 mV test pulse. (*Inset*) Mean τ_{DEACT} for the fluorescence (red) and ionic tail current (black) at −90 mV.

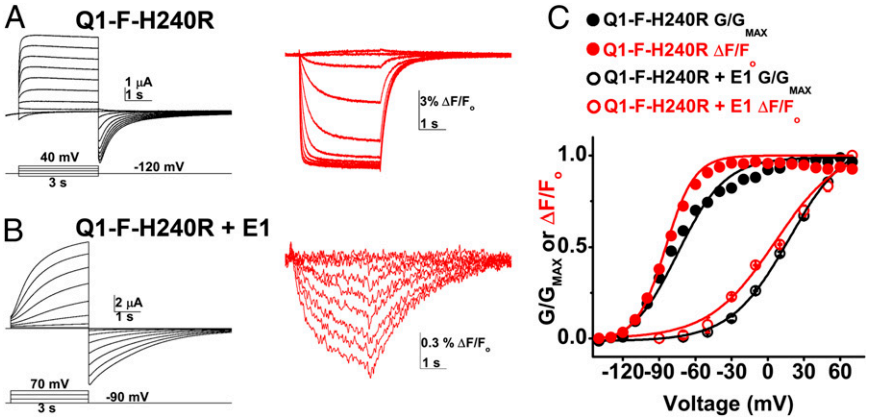

Fig. 6. E1 slows the movement of Q1-F-H240R voltage sensors. Ionic current and fluorescence signals were evoked simultaneously in cells expressing Q1-F-H240R or Q1-F-H240R + E1 channels and studied as in Fig. 4. Data are means ± SEM for three to seven cells in each group. (*A*) A representative family of ionic currents (*Left*) and fluorescence signals (*Right*) recorded in a cell expressing Q1-F-H240R channels, shown from −120 mV to 40 mV in 20-mV intervals. Cells were held at −90 mV and prepulsed to −120 mV for 1 s. (*B*) An exemplar family of ionic currents (*Left*) and fluorescence signals (*Right*) recorded in a cell expressing Q1-F-H240R + E1 channels. Shown from −90 to 70 mV in 20-mV intervals. (*C*) Mean, normalized fluorescence (F, red)-voltage and conductance (G, black)-voltage relationships for Q1-F-H240R (filled circles) and Q1-F-H240R + E1 (open circles) channels were measured after 3 s and fit as in Fig. 2; determined values are in Table 2.

Discussion

Here, we show that the difference in gating kinetics between Q1 channels and I_{Ks} channels is explained by E1-induced slowing of S4 segment movement. First, we demonstrate that Q1 channel gating currents can only be resolved in the absence of E1, implying that E1 subunits slow sensor movement. Next, we show close coupling of Q1 channel gating current and ionic currents, suggesting that S4 movement is rate-limiting for the opening of Q1 channel pores. Then, we assess SDF and ionic currents simultaneously to show that S4-segment fluorescent signals and ionic current kinetics coincide in the absence and presence of E1 subunits, supporting tight electromechanical coupling of sensor movement and pore opening. SDF shows directly that E1 slows S4 movement in I_{Ks} channels. Because E1 slows the activation of ionic currents and S4 movement to the same extent, we conclude that VSD movement is the rate-limiting step to the opening of channels and, therefore, that E1 is both necessary and sufficient to explain the slow kinetics of I_{Ks} channels.

Previously, the basis for slow activation of I_{Ks} channels was studied by two groups using the rate of MTS-modification of Cys residues introduced into the S4 segment of Q1 subunits. Nakajo and Kubo (27) reported the modification of one S4 site to be 10-fold slower in the presence of E1, suggesting an effect on voltage sensors. Rocheleau and Kobertz (28) observed E1 to slow modification of three sites; however, finding reaction rates to be independent of pulse duration they concluded that the S4 segments reached equilibrium quickly with membrane depolarization and the principal effect of E1 was to slow opening of the channel pore. In both cases, MTS-modification rate was used as a proxy for channel function, an indirect assay that is subject to confounding variables that have been well-enunciated (28).

Although Osteen et al. use SDF as we do here, they argue that E1 subunits impede both S4 movement and pore opening (29). We observe a direct correlation between fluorescence signals and ionic currents, indicating voltage sensor movements to be rate-limiting for activation of both Q1 and I_{Ks} channels, whereas they observe no such correlation for I_{Ks}. These discrepancies are likely to be the result of differences in experimental approach. Perhaps of greatest importance, we assessed SDF and ionic current simultaneously in the same cells because the activation of I_{Ks} differs from cell to cell (Fig. S6). In contrast, Osteen et al. do not compare fluorescence and ionic current simultaneously in the same cells, as different protocols are used and the two measurements made in different numbers of cells. Furthermore, we modified residue V221 to generate (Q1-F), a site that is 7 aa (~two helical turns) from the first conserved gating charge of the S4 transmembrane segment of Q1 (R1), and we used TMRM, a compact probe that links to V221C directly via a maleimide. In contrast, Osteen et al. studied G219, a site that is somewhat farther away from R1, and they used the larger fluorophore Alexa-488 with a five-carbon linker.

Engineering cysteine residues into the S3-S4 linker (and removing other natural residues) perturbs the biophysical features of Q1 channels, an issue noted in other studies (10, 27, 28, 36). We chose to study Q1-F after characterization supported its recapitulation of many salient features of Q1-WT. However, in common with the G219C variant used by Osteen et al. (29), we found that the *G-V* relationship of Q1-F channels was hyperpolarized with respect to Q1-WT (Table 2). We attempted to compensate for this shift with a pretest pulse step to a hyperpolarizing potential to close as many channels as possible; nonetheless, our conclusions must be cautioned to be based on studies of subunits bearing multiple mutations. In subsequent work, Osteen et al. propose models for Q1 channel operation that allow for transition between closed and open states before voltage-sensor movement (29, 37); we do not support these models based on our assessment of Q1-WT gating currents and our recording of ionic current activation lag (Fig. 2*E*) that they fail to observe.

Here, we are unique in reporting measurements of Q1 channel gating currents. As observed for other Kv channels, Q1 gating currents precede pore opening, occur at more hyperpolarized voltages than conductance, and deactivate more slowly than they activate. In contrast, the kinetics of Q1 gating currents are quite slow, activating ~fourfold less rapidly even than those measured for Q4 channels (and ~28-fold slower than Shaker channels) under similar conditions. Nonetheless, normalized *Q-V* curves for Q1 and Q4 channels superimpose (Fig. S2*C*), with $QV_{1/2}$ values ~20 mV more depolarized than those observed for Shaker channels studied under the same conditions (Table 1). The slope factors (z) of single Boltzmann fits of the *Q-V* relationships for Q1 and Q4 channels are smaller than that observed for Shaker. Although z in this case cannot be directly interpreted as the effective valence of the gating charge because gating does not correlate to a two-state model, this finding suggests a lower gating-charge

valence and may reflect the absence of the "R3" gating charge in Q1 and Q4 channels (Fig. 2*B*).

Applying a simplified two-state gating model for Q1, a z of 2.2 is consistent with 8–9 gating charges per channel, compared with 12–13 gating charges for Shaker channels (38–41). Assuming nine elementary gating charges per Q1 channel, a single-channel conductance of 4 pS (19) and the average integrated gating current and predepletion ionic current levels in Fig. 2, the open probability (P_O) of Q1 channels is estimated to ~0.004; a P_O of 0.07 was estimated for Q4 channels (42).

Our inability to measure gating currents for I_{Ks} channels was rationalized by the SDF studies that predict gating currents for Q1-WT + E1 channels would have a τ_{ACT} of ~1 s (Table 2), whereas the limit for resolving gating currents under the conditions we used was τ_{ACT} ~ 0.4 s (*Materials and Methods*). A decrease in gating-current amplitude can be caused by many nonkinetic factors, including traversal of a smaller fraction of the electric field, motion that is more tangential to the field, or a decrease in the number of gating charges. However, none of these factors could be reduced more than a few-fold and still produce a voltage-dependent channel, and we would have seen a small gating current had the signal amplitude decreased only a few-fold without a change in kinetics. Our SDF measurements confirm a dramatic sensor slowing that fully explains the disappearance of gating current with coexpression of E1. As gating currents were not resolved for I_{Ks} channels, an estimate for P_O cannot be calculated by the method used for Q1 channels. However, if the P_O for cardiac I_{Ks} channels is like that for Q1 channels in oocytes at 28 °C, it is interesting to ponder that during each human heartbeat, over 99.6% of I_{Ks} channels remain closed.

The slow gating of I_{Ks} channels is crucial to proper repolarization of cardiac myocytes and normal action potential duration. Hundreds of mutations have been identified in *KCNE1* and *KCNQ1* genes and many have been shown to alter ventricular repolarization and predispose to dangerous cardiac arrhythmias. Moreover, evidence is accumulating that Q1 assembles in vivo not only with E1 but also with the four minK-related peptides encoded by KCNE 2–5 to produce biophysically distinct channels (43–45). The strategies used here may help to reveal the impact of disease-associated mutations on I_{Ks} channels and expose how E1-5 act in channels with Q1 to yield channels with different attributes tailored to their tissues and roles in physiology.

Materials and Methods

Mutagenesis, Preparation of Oocytes, and Oocyte Labeling. Experiments were performed using wild-type human *KCNQ1* (Q1-WT) (NCBI ACC#NM_000218), *KCNQ1* H240R (Q1-WT-H240R), *KCNQ1* C214S V221C C331S (Q1-F), or *KCNQ1* C214S V221C H240R C331S (Q1-F-H240R) expressed with or without the wild-type human *KCNE1* (E1) (NCBI ACC#NP_000210.2). cDNAs were handled in an in-house vector, pRAT (46), and mutations introduced using QuikChange site-directed mutagenesis (Agilent Technologies). Plasmids were linearized with Xba1 (Q1) or Not1 (E1) restriction enzymes (New England Biolabs) and transcribed using T7 RNA polymerase (Life Technologies). Oocytes were harvested and prepared for COVC and SDF recordings as previously described (33, 47). Cells were injected with 12 ng Q1 with or without 6 ng E1 and incubated 3–5 d at 16 °C. For SDF cells were labeled in 120 K-MS, 0.05 mM EDTA, 10 mM Hepes, pH 7.4 with 20 μM TMRM (Life Technologies).

Electrophysiology. All recordings were performed at 28 °C by COVC (31) with a CA-1B amplifier (Dagan Corporation). The temperature was controlled as previously described (33). For ionic currents, the external solution comprised 4 mM K-MS, 111 mM *N*-methyl-D-glucamine (NMDG)-MS, 2 mM $Ca(MS)_2$, and 20 mM Hepes with 2 mM $Ba(MS)_2$ added where indicated. The internal solution was: 120 mM K-MS, 2 mM EGTA, and 20 mM Hepes. Pipettes were filled with 3 M KCl. For gating currents, cells were depleted of potassium ions as previously described (33). Gating currents were recorded in an external solution comprising 112 mM tetraethylammonium (TEA)-MS, 2 mM $Ca(MS)_2$, 2 mM $Ba(MS)_2$, and 20 mM Hepes; internal solution was 113 mM TEA-MS, 2 mM EGTA, and 20 mM Hepes. Pipettes were filled with 3 M CsMS and 20 mM CsCl. All solutions were adjusted to pH 7.4 with MS. Oocytes were permeabilized for COVC with 0.3% saponin. Microelectrodes had a resistance of 0.3 MΩ.

SDF Recordings. Oocytes expressed Q1-F or Q1-F-H240R channels, with or without E1, labeled with TMRM. Leak subtraction was not used. Prepulse and tail voltages were the same so an exponential fit to a fluorescence recording with no pulse applied could be subtracted from all fluorescence traces to account for bleaching. Ionic current and fluorescence were recorded simultaneously from each oocyte and paired data are reported. The setup has been described previously (47). For recordings with 3-s test pulses, the recorded signal was the integral of the fluorescence during the sampling interval of 2 ms.

Protocols and Data Analysis. Gating currents were recorded with the following protocol: from a holding potential of −90 mV, a 40-ms prepulse to −100 mV was followed by voltage steps from −100 mV to +40 mV (Q1-WT) or +60 mV (Q1-WT-H240R) for a duration of 300 ms (Q1-WT) or 150 ms (Q1-WT-H240R) before a final 600-ms step to −100 mV was applied. Gating currents were leak-subtracted online using a standard P/-8 protocol. Data were filtered at 2–5 KHz and sampled at 17 KHz. Gating-charge movement was obtained by integrating ON-gating current and OFF-gating current to obtain the time-course of Q_{ON} and Q_{OFF}, respectively. Ionic currents recorded using a 3-s test pulse were not leak subtracted. Ionic current data were filtered at 0.2–1 kHz and sampled at 0.5–3 kHz.

SDF data were sampled at 0.5 kHz and filtered at 5 kHz before being processed by an integrator circuit. For analysis of kinetics and superposition of ionic current and fluorescence, the small (<0.1% $\Delta F/F_o$) electrochromic rearrangement of the TMRM fluorescent probe was ignored (48). For superposition of SDF ionic current and fluorescence activation, ionic current was leak-subtracted offline using the assumption that channels are closed at −120 mV to compare only the kinetic component of the activating test pulse.

Conductance (G) was calculated from the tail current and expressed as G/G_{max} as a function of membrane voltage (G-V curves). Data were fit to the equation: $G = G_{max}/[1 + \exp(-zF(V - V_{1/2})/RT)]$ where V is the test potential, $V_{1/2}$ is the voltage of half-maximal activation, z is the effective valence, T is temperature, R is the gas constant, and F is the Faraday constant. Activation and deactivation kinetics were analyzed by fitting the current traces with a single- or double-exponential equation, as indicated, and are reported as the activation time-constant, τ_{ACT}, and deactivation time-constant, τ_{DEACT}, for the voltage of the corresponding trace (τ-V curves). Q was plotted as a function of membrane voltage (Q-V curves) and data were fit to the same equation as G. Q_{ON} and Q_{OFF} kinetics were obtained by fitting the integrated I_{gON} and I_{gOFF} traces, respectively, with a single exponential equation. Our SDF measurements predict Q1-WT + E1 channel gating currents will also have a τ_{ACT} of ~0.9 s. We conclude we are unable to resolve these gating currents because a gating current with τ_{ACT} of ~0.9 s and the intrinsic noise for a typical COVC gating current recording with the filter settings we used (~2.9 nA RMS) predict a signal/noise (S/N) ratio <1; we estimate that a time-constant of 0.4 s or faster, more than twice the τ_{ACT} predicted for Q1-WT + E1 based on SDF, is required to yield a S/N ratio of ~2.

Fluorescence values are reported as the change in fluorescence normalized by the initial level of fluorescence for each trace ($\Delta F/F_o$). The value of $\Delta F/F_o$ at the end of the activating test pulse is normalized to the maximal value and plotted with respect to the voltage of the test pulse (F-V curves). Fluorescence activation and deactivation kinetics were calculated as above. For figures showing a normalized superposition of open probability and gating charge or fluorescence, the normalized open probability is calculated either by dividing the ionic current by the instantaneous I-V relationship recorded in the same cell, or by normalizing the magnitude of each test pulse to the conductance value from the tail current. For each superposition, open probability and gating current or fluorescence are normalized to the most depolarized voltage shown in the series. Current and fluorescence data were recorded with an SB6711-based acquisition system with two parallel (nonmultiplexed) 16-bit A/D converters (Innovative Integration) with software written in-house. Analysis was also performed with software written in-house, with additional post hoc analysis performed using Clampfit (Molecular Devices), and Matlab (MathWorks). Data are expressed as the mean ± the SEM. All chemicals were obtained from Sigma-Aldrich, unless otherwise stated.

ACKNOWLEDGMENTS. The authors thank L. Plant and D. Goldstein for dedicated support during the course of this work. This work was funded in part by National Institutes of Health Grants R01HL105959 (to S.A.N.G.), R01GM030376 (to F.B.), T32GM7281, and The Paul and Daisy Soros Fellowship for New Americans (to K.J.R.).

1. Takumi T, Ohkubo H, Nakanishi S (1988) Cloning of a membrane protein that induces a slow voltage-gated potassium current. *Science* 242(4881):1042–1045.
2. Goldstein SA, Miller C (1991) Site-specific mutations in a minimal voltage-dependent K^+ channel alter ion selectivity and open-channel block. *Neuron* 7(3): 403–408.
3. Blumenthal EM, Kaczmarek LK (1994) The minK potassium channel exists in functional and nonfunctional forms when expressed in the plasma membrane of *Xenopus* oocytes. *J Neurosci* 14(5 Pt 2):3097–3105.
4. Tai K-K, Wang K-W, Goldstein SAN (1997) MinK potassium channels are heteromultimeric complexes. *J Biol Chem* 272(3):1654–1658.
5. Barhanin J, et al. (1996) K(V)LQT1 and IsK (minK) proteins associate to form the I(Ks) cardiac potassium current. *Nature* 384(6604):78–80.
6. Sanguinetti MC, et al. (1996) Coassembly of K(V)LQT1 and minK (IsK) proteins to form cardiac $I_{(Ks)}$ potassium channel. *Nature* 384(6604):80–83.
7. Splawski I, Tristani-Firouzi M, Lehmann MH, Sanguinetti MC, Keating MT (1997) Mutations in the hminK gene cause long QT syndrome and suppress I_{Ks} function. *Nat Genet* 17(3):338–340.
8. Splawski I, Timothy KW, Vincent GM, Atkinson DL, Keating MT (1997) Molecular basis of the long-QT syndrome associated with deafness. *N Engl J Med* 336(22):1562–1567.
9. Chen H, Kim LA, Rajan S, Xu S, Goldstein SA (2003) Charybdotoxin binding in the $I_{(Ks)}$ pore demonstrates two MinK subunits in each channel complex. *Neuron* 40(1):15–23.
10. Panaghie G, Abbott GW (2007) The role of S4 charges in voltage-dependent and voltage-independent KCNQ1 potassium channel complexes. *J Gen Physiol* 129(2): 121–133.
11. Abbott GW, Goldstein SAN (1998) A superfamily of small potassium channel subunits: Form and function of the MinK-related peptides (MiRPs). *Q Rev Biophys* 31(4): 357–398.
12. Abbott GW, et al. (1999) MiRP1 forms IKr potassium channels with HERG and is associated with cardiac arrhythmia. *Cell* 97(2):175–187.
13. Abbott GW, et al. (2001) MiRP2 forms potassium channels in skeletal muscle with Kv3.4 and is associated with periodic paralysis. *Cell* 104(2):217–231.
14. Abbott GW, Goldstein SA (2002) Disease-associated mutations in KCNE potassium channel subunits (MiRPs) reveal promiscuous disruption of multiple currents and conservation of mechanism. *FASEB J* 16(3):390–400.
15. Wang KW, Goldstein SAN (1995) Subunit composition of minK potassium channels. *Neuron* 14(6):1303–1309.
16. Morin TJ, Kobertz WR (2008) Counting membrane-embedded KCNE β-subunits in functioning K+ channel complexes. *Proc Natl Acad Sci USA* 105(5):1478–1482.
17. Nakajo K, Ulbrich MH, Kubo Y, Isacoff EY (2010) Stoichiometry of the KCNQ1–KCNE1 ion channel complex. *Proc Natl Acad Sci USA* 107(44):18862–18867.
18. Wang K-W, Tai K-K, Goldstein SAN (1996) MinK residues line a potassium channel pore. *Neuron* 16(3):571–577.
19. Sesti F, Goldstein SAN (1998) Single-channel characteristics of wild-type I_{Ks} channels and channels formed with two minK mutants that cause long QT syndrome. *J Gen Physiol* 112(6):651–663.
20. Tai KK, Goldstein SAN (1998) The conduction pore of a cardiac potassium channel. *Nature* 391(6667):605–608.
21. Tristani-Firouzi M, Sanguinetti MC (1998) Voltage-dependent inactivation of the human K+ channel KvLQT1 is eliminated by association with minimal K+ channel (minK) subunits. *J Physiol* 510(Pt 1):37–45.
22. Sesti F, Tai KK, Goldstein SAN (2000) MinK endows the I_{Ks} potassium channel with sensitivity to internal TEA. *Biophys J* 79(3):1369–1378.
23. Chen H, Sesti F, Goldstein SAN (2003) Pore- and state-dependent cadmium block of I $(_{Ks})$ channels formed with MinK-55C and wild-type KCNQ1 subunits. *Biophys J* 84(6): 3679–3689.
24. Melman YF, Um SY, Krumerman A, Kagan A, McDonald TV (2004) KCNE1 binds to the KCNQ1 pore to regulate potassium channel activity. *Neuron* 42(6):927–937.
25. Chen H, Goldstein SAN (2007) Serial perturbation of MinK in IKs implies an α-helical transmembrane span traversing the channel corpus. *Biophys J* 93(7):2332–2340.
26. Kang C, et al. (2008) Structure of KCNE1 and implications for how it modulates the KCNQ1 potassium channel. *Biochemistry* 47(31):7999–8006.
27. Nakajo K, Kubo Y (2007) KCNE1 and KCNE3 stabilize and/or slow voltage sensing S4 segment of KCNQ1 channel. *J Gen Physiol* 130(3):269–281.
28. Rocheleau JM, Kobertz WR (2008) KCNE peptides differently affect voltage sensor equilibrium and equilibration rates in KCNQ1 K+ channels. *J Gen Physiol* 131(1):59–68.
29. Osteen JD, et al. (2010) KCNE1 alters the voltage sensor movements necessary to open the KCNQ1 channel gate. *Proc Natl Acad Sci USA* 107(52):22710–22715.
30. Armstrong CM, Bezanilla F (1973) Currents related to movement of the gating particles of the sodium channels. *Nature* 242(5398):459–461.
31. Stefani E, Bezanilla F (1998) Cut-open oocyte voltage-clamp technique. *Methods Enzymol* 293:300–318.
32. Cha A, Bezanilla F (1998) Structural implications of fluorescence quenching in the Shaker K+ channel. *J Gen Physiol* 112(4):391–408.
33. Miceli F, et al. (2009) Gating currents from neuronal Kv7.4 channels: General features and correlation with the ionic conductance. *Channels* 3(4):277–286.
34. Bezanilla F, Perozo E, Papazian DM, Stefani E (1991) Molecular basis of gating charge immobilization in Shaker potassium channels. *Science* 254(5032):679–683.
35. Labro AJ, Lacroix JJ, Villalba-Galea CA, Snyders DJ, Bezanilla F (2012) Molecular mechanism for depolarization-induced modulation of Kv channel closure. *J Gen Physiol* 140(5):481–493.
36. Haitin Y, et al. (2008) S1 constrains S4 in the voltage sensor domain of Kv7.1 K+ channels. *PLoS One* 3(4):e1935.
37. Osteen JD, et al. (2012) Allosteric gating mechanism underlies the flexible gating of KCNQ1 potassium channels. *Proc Natl Acad Sci USA* 109(18):7103–7108.
38. Schoppa NE, McCormack K, Tanouye MA, Sigworth FJ (1992) The size of gating charge in wild-type and mutant Shaker potassium channels. *Science* 255(5052):1712–1715.
39. Aggarwal SK, MacKinnon R (1996) Contribution of the S4 segment to gating charge in the Shaker K^+ channel. *Neuron* 16(6):1169–1177.
40. Noceti F, et al. (1996) Effective gating charges per channel in voltage-dependent K+ and Ca2+ channels. *J Gen Physiol* 108(3):143–155.
41. Seoh S-A, Sigg D, Papazian DM, Bezanilla F (1996) Voltage-sensing residues in the S2 and S4 segments of the Shaker K+ channel. *Neuron* 16(6):1159–1167.
42. Li Y, Gamper N, Shapiro MS (2004) Single-channel analysis of KCNQ K+ channels reveals the mechanism of augmentation by a cysteine-modifying reagent. *J Neurosci* 24(22):5079–5090.
43. Schroeder BC, et al. (2000) A constitutively open potassium channel formed by KCNQ1 and KCNE3. *Nature* 403(6766):196–199.
44. Tinel N, Diochot S, Borsotto M, Lazdunski M, Barhanin J (2000) KCNE2 confers background current characteristics to the cardiac KCNQ1 potassium channel. *EMBO J* 19(23):6326–6330.
45. Jespersen T, Grunnet M, Olesen S-P (2005) The KCNQ1 potassium channel: From gene to physiological function. *Physiology (Bethesda)* 20(6):408–416.
46. Rajan S, Plant LD, Rabin ML, Butler MH, Goldstein SA (2005) Sumoylation silences the plasma membrane leak K^+ channel K2P1. *Cell* 121(1):37–47.
47. Villalba-Galea CA, Sandtner W, Starace DM, Bezanilla F (2008) S4-based voltage sensors have three major conformations. *Proc Natl Acad Sci USA* 105(46):17600–17607.
48. Asamoah OK, Wuskell JP, Loew LM, Bezanilla F (2003) A fluorometric approach to local electric field measurements in a voltage-gated ion channel. *Neuron* 37(1):85–97.